Article

Extraction and Modification of Cellulose Microfibers Derived from Biomass of the Amazon *Ochroma pyramidale* Fruit

Ana Luisa Farias Rocha [1], Bianca de Andrade Feitosa [2], Adriano de Souza Carolino [1],
Ronald Zico de Aguiar Nunes [1,*], Célio Matias Airone Macalia [1], Kalil Araújo da Silva [1],
Cleverton Oliveira Dias [3], Sérgio Michielon de Souza [3], Pedro Henrique Campelo [4],
Jaqueline de Araújo Bezerra [5] and Edgar Aparecido Sanches [1,3,*]

1 Laboratory Yvonne Mascarenhas (LabYM), Federal University of Amazonas (UFAM),
Manaus 69067-005, AM, Brazil
2 School of Engineering of São Carlos, University of São Paulo (USP), São Carlos 13566-590, SP, Brazil
3 Graduation Program in Physics (PPGFIS), Federal University of Amazonas (UFAM),
Manaus 69067-005, AM, Brazil
4 Department of Food Technology, Federal University of Viçosa (UFV), Viçosa 36570-900, MG, Brazil
5 Analytical Center, Federal Institute of Education, Science and Technology of Amazonas (IFAM),
Manaus 69020-120, AM, Brazil
* Correspondence: ronaldzico14@gmail.com (R.Z.d.A.N.); sanchesufam@ufam.edu.br (E.A.S.)

Abstract: Microfibers are important to several areas of human lifestyle, and the knowledge about
their physicochemical characteristics allows for proposing new technological applications. The *in
natura* microfiber of *Ochroma pyramidale* fruit (IN sample) and its extracted pulp (PU sample) were
evaluated by X-ray Diffraction (XRD), Scanning Electron Microscopy (SEM), Fourier Transform In-
frared Spectroscopy (FTIR) and Thermogravimetry and Differential Scanning Calorimetry (TG/*d*TG
and DSC). Microfibers were composed mainly of (68 ± 1)% holocellulose, (35.8 ± 0.1)% cellulose,
(32 ± 3)% lignin and (3.7 ± 0.3)% extractives. The XRD pattern of the PU sample revealed that
the mercerization process resulted in the change of the cellulose crystal structure from Iα type (tri-
clinic) to type II (monoclinic). The SEM technique showed that the IN sample presented regular
cylindrical/hollow-shaped wire-like microfibers with diameters ranging from 5 μm to 25 μm. How-
ever, the mercerization process changed their natural morphology. A significant change in the FTIR
spectra after the removal of hemicellulose and lignin components was observed: weak bands at
1739 cm^{-1} (C=O stretching of lignin and hemicellulose fractions), 1463 cm^{-1} (CH$_3$ of lignin) and
1246 cm^{-1} (C-O of lignin) were still observed in the PU sample, indicating that the lignin was not
completely removed due to the natural difficulty of isolating pure cellulose. The TG/*d*TG and DSC
evaluation revealed a temperature increase of the second thermal event (starting at 235 °C) in the PU
sample, which was assigned to the cellulose and residual hemicellulose degradation. Then, this work
aimed to disseminate and characterize a microfiber with unusual characteristics still little explored
by the scientific community, as well as its cellulosic pulp, providing information that may be useful
in its application in different industries, enabling the positive development of new biocompatible,
renewable and sustainable materials.

Keywords: *Ochroma pyramidale*; amazon microfiber; cellulose; hemicellulose; lignocellulosic microfiber

1. Introduction

The demand for sustainable and environmentally friendly products has been increas-
ingly becoming a new global concern. In this context, lignocellulosic sources have been
considered an alternative material to nondegradable fossil-fuel-based polymers due to its
abundance and biodegradability, as well as renewability, large specific surface area, low
cost and rich chemical functional groups [1,2]. Cellulose represents the major compound of
the lignocellulosic biomass, as well as the most abundant natural biopolymer. The chemical

structure of cellulose is constituted of β-1,4-linked glucopyranose units, which bear three hydroxyl groups. The search for friendly materials has made cellulose one of the most studied natural polymers, especially because it can be extracted from a variety of sources and crystal structures [3,4].

Ochroma pyramidale (Cav. ex Lamb.) Urban, known in Brazil as "pau-de-balsa", is a Malvaceae specie widely distributed from southern Mexico to Bolivia and Brazilian Amazon rainforest, and is well known for its low-density wood. It can reach 25 m in height and 1.2 m in diameter. Its flowers appear in the rainy season (April–July) and the fruits in the dry season (July–October). Figure 1a shows the *O. pyramidale* fruits, which are loculicidal, almost cylindrical, ligneous and dehiscent. These fruits present a very soft yellow-brown inner fiber (Figure 1b), which promotes the dispersion of seeds by the wind [5]. Reports on *O. pyramidale* have usually considered its wood [6–8], seed germination [9], or use for reforestation due to its fast growth [6,10]. Furthermore, some works also have reported its use as filling for beds, pillows and lifeguards due to its softness and buoyancy [11]. On the other hand, another specie from the same family known as kapok (*Ceiba pentandra* L.) also presents a fruit with extremely similar morphological fiber. Reports are giving attention to its application as biofuels [12,13], oil absorbents [11,14,15], acoustic and thermal insulation [11,16], thermoplastic composites [17], paper and textile yield, polymeric matrix and even drug release [18], suggesting similar application potential of *O. pyramidale* [16].
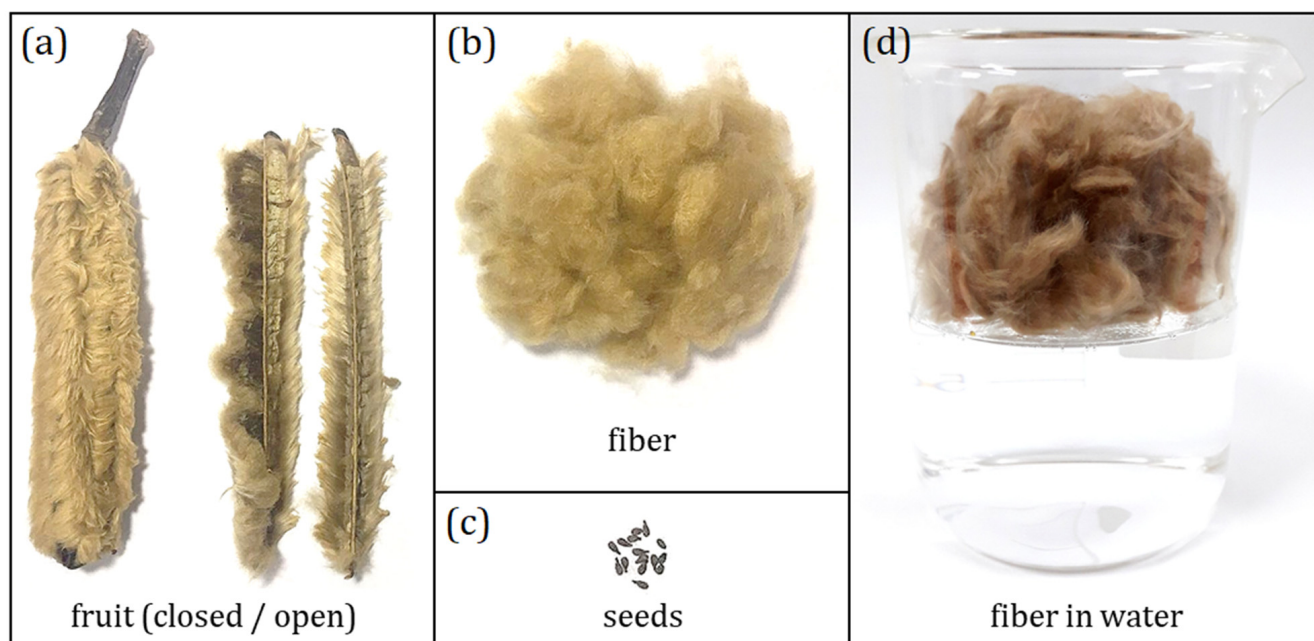
Figure 1. Parts composing the *O. pyramidale* fruits: (**a**) whole fruit, (**b**) fibers and (**c**) seeds; and (**d**) fibers in water.

Lignocellulosic fibers have been extensively evaluated as reinforcement in thermoplastic, polymeric composites and composites for building [1,19–21], oil adsorbents [22,23], bioplastics [24], biofilters [25], biofuel [26], acoustic and thermal insulators [27,28], chemical products and cosmetic [2] and biomedical application [3,29,30]. The study of new fibers represents an important topic of research due to the possibility of proposing new technological applications. In this context, producing new data about *O. pyramidale* fruit fibers proves to be a good proposal. For this reason, the aim of this paper was to perform a systematic physicochemical, structural, morphological and thermal investigation of the *O. pyramidale* fruit fibers: X-ray Diffraction technique (XRD) was applied in order to examine the long-range order achieved as a consequence of very short-range interactions. Fourier Transform Infrared Spectroscopy (FTIR) was applied for molecular structural characterization, as well

as to confirm the success of the proposed method of cellulose extraction. Scanning Electron Microscopy (SEM) was useful to assess the fibers' morphology. Finally, Thermogravimetric analysis (TG/dTG) and Differential Scanning Calorimetry (DSC) were conducted to evaluate the thermal stability of the fibers and pulp extracted from the Amazon *Ochroma pyramidale* fruit.

2. Experimental

2.1. Materials

Plant Material

O. pyramidale fruits (SISGEN n° A26CD5E) were collected at the Instituto Federal de Educação, Ciência e Tecnologia do Amazonas (IFAM)—Campus Zona Leste, Manaus/AM (3°4′51.8268 S and 59°56′2.9328 W). Fibers *in natura* were separated from seeds and maintained at 25 °C until further analysis (labeled as IN sample). Botanical identification was carried out at the Federal University of Amazonas (UFAM) following the established protocol.

2.2. Methods

2.2.1. Physicochemical Composition

The physicochemical composition of the IN sample was performed according to adapted TAPPI methodologies [31]. All measurements were performed in triplicate.

To measure the Moisture Content (M%), 2 g (m_i) of the IN sample were submitted to a thermal treatment in an oven at 105 °C for 3 h, according to TAPPI 412 om-16 [31]. M% was determined by Equation (1):

$$\left(\frac{m_i - m_f}{m_i}\right) \times 100 = M\% \tag{1}$$

where m_i and m_f represent, respectively, the initial and final mass of the IN sample.

An amount of 0.3 g (m_i) of dried IN sample was carbonized in an industrial oven on asbestos leaf for 1 h. Then, the resulting material was placed in a muffle under a heating rate of 9.6 °C/min for 3 h up to 600 °C to measure the Ash Content (A%) [32]. A% was determined by Equation (2):

$$\left(\frac{m_a}{m_i}\right) \times 100 = A\% \tag{2}$$

where m_a represents the mass of ashes.

For Cold-Water Solubility (CW%) measurement, 2 g of dried IN sample were added in water (300 mL) at 25 °C for 48 h under constant stirring and then washed with 200 mL of distilled water and filtered. For the Hot-Water Solubility (HW%) measurement, 2 g of dried IN sample were added in boiling water (200 mL) for 3 h, washed with 200 mL of boiling distilled water and filtered. Both water-treated fibers were placed in an oven at 103 °C until they reached constant weight [33]. Then, the CW% and HW% were determined by Equation (1).

To remove and evaluate the Extractives Content (E%) as a previous process, 4 g of dried IN sample were submitted to solvent extraction using a Soxhlet system using 180 mL of ethanol and acetone 2:1 at 70 °C for 4 h. The solvent with extractives was dried in an oven at 105 °C until constant weight. E% was determined according to Equation (2), but considering the mass of extractives, and the Extractives Content Corrected (E_{cor}%) was measured following Equation (3) [34]. Then, the treated and dried fibers were submitted to the extraction of holocellulose, cellulose and lignin.

$$\left(\frac{E\% \times (100 - M\%)}{100}\right) = E_{cor}\% \tag{3}$$

To determine the Lignin Content (L%), 1 g (m_i) of treated fibers (without moisture and extractives) was added to H_2SO_4 (17 mL, 72% *v/v*) for 24 h at 25 °C. Then, the system was

diluted to 4% using distilled water and agitated at 70 °C for 4 h. The resulting material was filtered using a sintered filter type 3 and maintained in an oven at 105 °C until constant weight [35]. *L%* was determined according to Equation (4), and Lignin Content Corrected (L_{cor}%) was measured following Equation (5):

$$\left(\frac{m_{lig}}{m_i} \times 100 \right) - A\% = L\% \tag{4}$$

$$\left(\frac{L\% \times [100 - (M\% + E_{cor}\%)]}{100} \right) = L_{cor}\% \tag{5}$$

where m_{lig} represents the mass of lignin.

To determine Holocellulose Corrected (Ho_{cor}%), Hemicellulose Corrected (He_{cor}%) and Cellulose Corrected (C_{cor}%) contents, 3 g of the treated fibers (without moisture or extractives) were submitted to a system containing $NaClO_2$ (5 g) and CH_3COOH (2 mL) in distilled water (240 mL) at 70 °C for 1 h for oxidation of lignin and reapplied for another hour aiming the obtainment of holocellulose. Then, 1 g of the obtained holocellulose (m_{ho}) was submitted to NaOH (15 mL, 17.5% m/m, 10 min) under maceration, and then distilled water (40 mL) was added. The final solution was filtered on a sintered filter type 2 to obtain the pulp material (labeled as PU sample) [36]. The obtained holocellulose and cellulose were dried in an oven at 105 °C until constant weight. Ho% and Ho_{cor}% were determined according to Equations (2) and (5), respectively. C%, C_{cor}% and He_{cor}% were measured using the following equations:

$$\left(\frac{m_c}{m_{ho}} \right) \times 100 = C\% \tag{6}$$

$$\left(\frac{Ho_{cor}\% \times C\%}{100} \right) = C_{cor}\% \tag{7}$$

$$Ho_{cor}\% - C_{cor}\% = He_{cor}\% \tag{8}$$

where m_{ho}, m_c and He_{cor}% represent, respectively, the mass of holocellulose, mass of cellulose and Hemicellulose Content Corrected.

2.2.2. X-ray Diffraction (XRD) and Percentage of Crystallinity

X-ray diffraction technique (XRD) was performed on a Panalytical Empyrean diffractometer, CuK_{α}, 40 kV and 40 mA. Measurements were performed using a Si single-crystal sample holder from 5° to 100° (2θ), step of 0.01313° and 5 s/step. A LaB_6 standard NIST (660 b) was used to consider the instrumental effects. The Rietveld method implemented in the GSAS-2 software package was used to refine structural parameters and line widths, following the recommendations of IUCr [37]. Crystal data of cellulose polymorphs I_{α} (triclinic; a = 10.400 Å; b = 6.717 Å; c = 5.962 Å; α = 80.370°; β = 118.080° and γ = 114.800°) [38] and type II (monoclinic; a = 8.100 Å; b = 9.030 Å; c = 10.310 Å; α = 90°; β = 90° and γ = 117.100°) [39] were considered as initial parameters. The percentage of crystallinity was measured using the deconvolution method [40,41].

2.2.3. Scanning Electron Microscopy (SEM)

SEM experiments were performed on a Carl Zeiss equipment model Supra 35, using 1.0 kV at 25 °C. Samples were placed on carbon tape and covered with a thin gold layer prior to analysis. The fiber diameter distribution was determined using the software ImageJ 1.53 t [42] and statistical program OriginPro 8® [43] considering 500 units of IN sample.

2.2.4. Fourier Transform Infrared Spectroscopy (FTIR)

FTIR spectrum was recorded using a Shimadzu IR Prestige-21 Spectrometer TA Instruments® from 4000 to 400 cm^{-1}, resolution of 1 cm^{-1} and 64 scans.

2.2.5. Thermogravimetry/Derivative Thermogravimetry (TG/dTG) and Differential Scanning Calorimetry (DSC)

TG/dTG and DSC techniques were performed on a SDT Q600 TA Instruments at the Laboratório de Materiais da Amazônia e Compósitos (LaMAC-FT/UFAM). Measurements were carried out using approximately 5.5 mg of samples in alumina crucibles, N_2 atmosphere (flow of 30 mL/min) at a heating rate of 10 °C/min, from 20 °C to 600 °C.

2.2.6. Thermal Conductivity

The TCi equipment, developed by the C-Therm Company, Fredericton, NB, Canada, was utilized to perform thermal conductivity measurements. This equipment employs the modified transient plane source (MTPS) method to determine the thermal conductivity of the sample. The measurements were conducted at room temperature, and microfibers served as the reference material in all instances. The correlation factor R^2, which assesses the agreement between the experimental results and the reference material, approached 99%.

3. Results and Discussion

3.1. Physicochemical Characterization

Figure 1 shows the parts composing the *O. pyramidale* fruits, including their microfibers and seeds. Structural and nonstructural compounds were extracted from their microfibers and quantified.

Table 1 shows the main percentual compounds of the IN sample and other wood and nonwood values for comparation. The values shown are the corrected contents.

Holocellulose (Ho%) considers the sum of hemicellulose and cellulose. A value of (68 ± 1)% was obtained, which was similar to those found in *E. binata* (64%) [44], *P. dactylifera* (70%) [45] and *H. sabdariffa* (74%) [46]. The presence of hemicellulose in a bleached sample may be useful depending on the purpose and can be an alternative to the pure cellulose due to its easier obtention, lower cost and higher yield. Purnawati et al. 2018 [16] and Prachayawarakorn et al. 2013 [17] obtained Ho% values higher than 80% in balsa and kapok fruit fibers. On the other hand, the cellulose value of (35.8 ± 0.1)% represented one of the smallest values shown in Table 1, but similar to those found in *C. pentandra* (38.09%) [16], *C. nucifera* (35.62%) [23] and *P. dactylifera* (35–44%) [45]. The L% value was found around (32 ± 3)%, which was almost double the value found in balsa fruit [16] and one of the highest lignin values shown in Table 1. This characteristic assures its high hydrophobicity acting synergically with the extractives, as observed in Figure 1d. The difference between values from Table 1 can be explained, because these natural constituents are significantly related to the soil type, weather, plant age, harvest, maturation, presence of pests or diseases as well as methods of extraction, reagents and manipulation [47–49]. The A% value (2.03 ± 0.03)% agrees with that found for the residual mass obtained through TG/dTG analysis.

The *O. pyramidale* fruit fiber presented a surface constituted of extractives (E% = 3.7 $\pm$ 0.3) [16] based on secondary metabolites. Despite presenting a low concentration of extractives, their association to lignin allows for a hydrophobic–lipophilic fiber's property [15,17] preventing their interaction to water [50]. Similar behavior was observed in kapok fibers [15]. This information is consistent with their role in nature: the high concentration of secondary metabolites is not necessary, because their function, as far as we know, is just to disperse their seeds by the wind.

Considering the use of nonlipophilic fibers for oleophilic purposes, a chemical surface modification might be applied [14]. However, in the case of *O. pyramidale* and *C. pentandra* fruit fibers, this modification may not be necessary, representing an important advantage when compared to other plant fibers.

Purnawati et al. 2018 [16] performed the fiber's wettability analysis and obtained angles higher than 118°, confirming their high hydrophobicity. On the other hand, through CW% (7.5 $\pm$ 0.6%) and HW% (8.4 $\pm$ 0.2%) treatments performed in this present work, a

slight solubility was suggested, but not identified in the immediate contact fibers water, requiring the use of a mechanic (CW%) or thermal action (HW%).

Table 1. Main compounds of the *O. pyramidale* fibers (in natura) compared to other wood and nonwood sources.

Specie	M%	E%	He%	C%	L%	A%	Reference
Balsa fruit fiber (*Ochroma pyramidale*)	8.7 ± 0.2	3.7 ± 0.3	33 ± 1	35.8 ± 0.1	32 ± 3	2.04 ± 0.03	(Present work)
Balsa fruit fiber (*Ochroma pyramidale*)	11.45	2.29	37.35	44.62	16.6	0.94	[16]
Kapok fruit fiber (*Ceiba pentandra*)	11.23	2.34	45.64	38.09	14.1	1.05	[16]
Kapok bark (*Ceiba pentandra*)	7.46	0.38	17.53	60.9	23.5	1.05	[51]
Kapok fruit fiber (*Ceiba pentandra*)	–	23	23	64	19	–	[17]
Coconut fiber (*Cocos nucifera*)	–	–	8.51	35.62	37.59	0.97	[23]
Jute stem (*Corchorus capsularis*)	–	0.5	14–20	61–71	12–13	–	[51]
Sisal leaf (*Agave sisalana*)	–	2	12	65	9.9	–	[51]
Kenaf stem (*Hibiscus cannabinus*)	–	0.3	20.3	72	9	–	[51]
Oil palm leaves (*Elaeis guineensis*)	–	–	34	42.67	22.9	–	[51]
Umbrella thorn bark (*Acacia tortilis*)	6.47	17.43	–	61.89	21.26	4.33	[1]
Buriti leaf fiber (*Mauritia flexuosa*)	9	6	1	58	19	2	[19]
Date palm (*Phoenix dactylifera*)	5.4–15.6	–	9.75–26	35–44	11–29	3–12	[45]
Sabai grass (*Eulaliopsis binata*)	–	–	21.1	42.9	18.5	13.4	[44]
Portia tree bark (*Thepesia populnea*)	9.8–11.5	0.7–0.8	12–16	64–70	16–18	1.7–2.1	[52]
Roselle stems (*Hibiscus sabdariffa*)	–	–	16–20	58–64	6–10	–	[46]

3.2. XRD Analysis

XRD analysis was carried out as a tool to investigate the crystal structure of both IN and PU samples. Figure 2a,b shows the overlapped diffraction patterns.

Cellulose polymorphism has been associated with the source and extraction method [53,54]. The cellulose polymorph in most plants is generally Iβ type (monoclinic) [52], but both Iα and Iβ polymorphs can coexist in this material, presenting diffraction peaks at similar angular positions. Therefore, depending on the chemical procedure, some extracted cellulose can also present the Iα type (triclinic) after refinement, as previously reported [53].
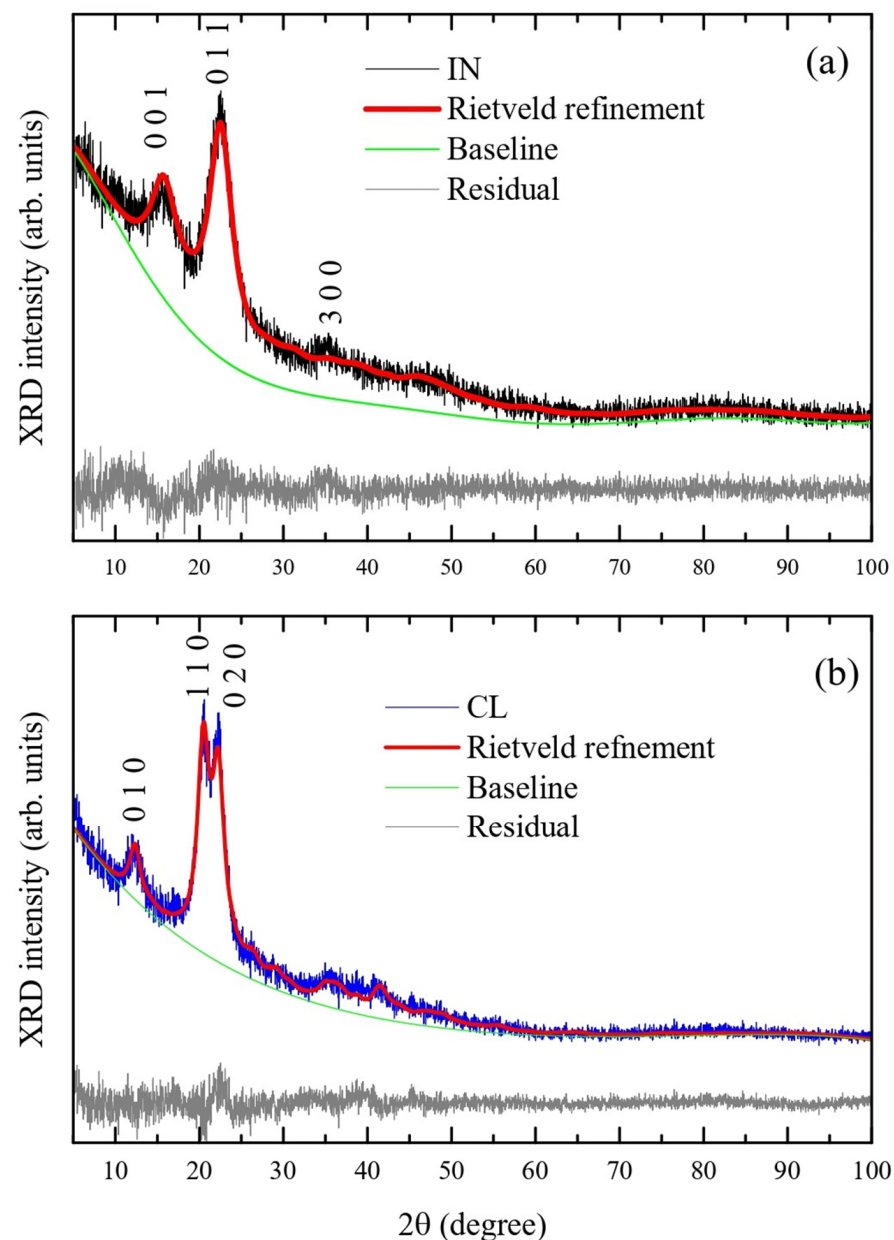
Figure 2. XRD patterns of (**a**) IN and (**b**) PU samples.

All XRD measurements were performed under the same experimental conditions. Thus, the differences between the intensities of the XRD patterns were attributed to different crystallinity levels. Despite presenting lignin, hemicellulose and partial cellulose as noncrystalline phases, the IN sample also presented the contribution of the crystalline cellulose phase. Naturally, bulk cellulose consists of highly ordered, crystalline regions disposed along disordered (amorphous/noncrystalline) regions in varying proportions, which depends on the cellulose source [55].

The XRD pattern of the IN sample was accurately represented by the Iα type cellulose (triclinic) [16]. The peaks located at 15.9°, 22.4° and 35.5° (2θ) were related to (001), (011) and (300) plans, respectively (Figure 2a). However, the XRD pattern of the PU sample (Figure 2b) presented a considerable phase changing. The peaks located at 12°, 20° and 22° corresponded, respectively, to (010), (110) and (020) plans. The mercerization process has been considered an irreversible method to extract cellulose able to change its crystal structure. In our case, the cellulose crystal structure Iα changed to type II (monoclinic) [24,54]. Table 2 shows the lattice parameters obtained by the Rietveld refinement.

Table 2. Cell parameters obtained from Rietveld refinement.

	IN Sample [38]	IN Sample	PU Sample [39]	PU Sample
a (Å)	10.4	10.49 ± 0.06	8.10	7.87 ± 0.01
b (Å)	6.717	6.74 ± 0.03	9.03	9.01 ± 0.01
c (Å)	5.962	6.26 ± 0.02	10.31	10.19 ± 0.02
α (°)	80.37	76.3 ± 0.3	90	90
β (°)	118.08	112.5 ± 0.4	90	90
γ (°)	114.8	127.4 ± 0.2	117.1	117.77 ± 0.07
Volume (Å^3)	-	325 ± 2	-	641 ± 2
χ^2	-	1.104	-	1.205
R_{wp} (%)	-	0.0862	-	0.1091

The percentage of crystallinity of the PU sample was estimated using the deconvolution method. A value of 87% was estimated, which was similar to that found in a previous report [56], suggesting that the alkaline pretreatment considerably removed the noncrystalline contribution [57]. However, this method was not applied to estimate the crystallinity of the IN sample due to the air- scattering and their noncrystalline structural components, which may influence the XRD pattern.

3.3. Morphological Analysis

The SEM technique was performed to investigate the surface morphology of both IN and PU samples. Figure 3a,b shows that the IN sample presented a regular wire-like shape with a smooth surface. The large fiber's length size did not accurately allow their measurements. However, [16] reported their range from 10.36 nm to 15.7 mm. The IN sample presented diameters ranging from 5 μm to 25 μm (with average diameter of 15 μm). Furthermore, Figure 3c,d shows that the IN sample presented a tube-like morphology, characterized by its cylindrical/hollow shape and slightly roughened inner surface. The high percentage of lignin may be responsible for the observed cylindrical/hollow morphology due to its role in the support of vegetable wall cell structure [47,58]. Figure 3e,f shows the fiber's morphology after rupture, showing well-defined and interconnected microfibrils of cellulose composing the tubes. This morphology is similar to that of kapok fruit fibers [11,14,18], described previously as a hollow tube with porosity around 80% [15]. This characteristic can differentiate it from other vegetable fibers, which are generally massive but porous-like sponges.

The removal of lignin, hemicellulose and other components by bleaching treatment can be observed in the PU sample (Figure 4a,b). Fibers lost their original cylindrical/hollow morphology (as shown in Figure 4c,d), exposing their rough surface (Figure 4e,f) in a random-fold fashion. This characteristic is similar to that of cellulose reported previously [46,59]. Different methods of cellulose extraction have been proposed, showing their influence on the material surface [60] and physicochemical properties, as is also observed in the present work.

3.4. FTIR Analysis

Figure 5 shows the FTIR spectra of both IN and PU samples and the summarized peaks are at Table 3. The bands resulting from the chemical bonds of the IN sample were observed (considering all lignocellulosic components). A significant change in the spectral profile of the PU sample after the removal of hemicellulose and lignin components was observed.

Bands related to the –OH vibration were observed around 3500 cm^{-1}, which may result from the presence of water associated with the free hydroxyl groups in the main

chain of cellulose [61]. The main region of interest in lignocellulosic materials ranged from 1800 cm^{-1} to 800 cm^{-1}, where the main characteristic bands are usually located.
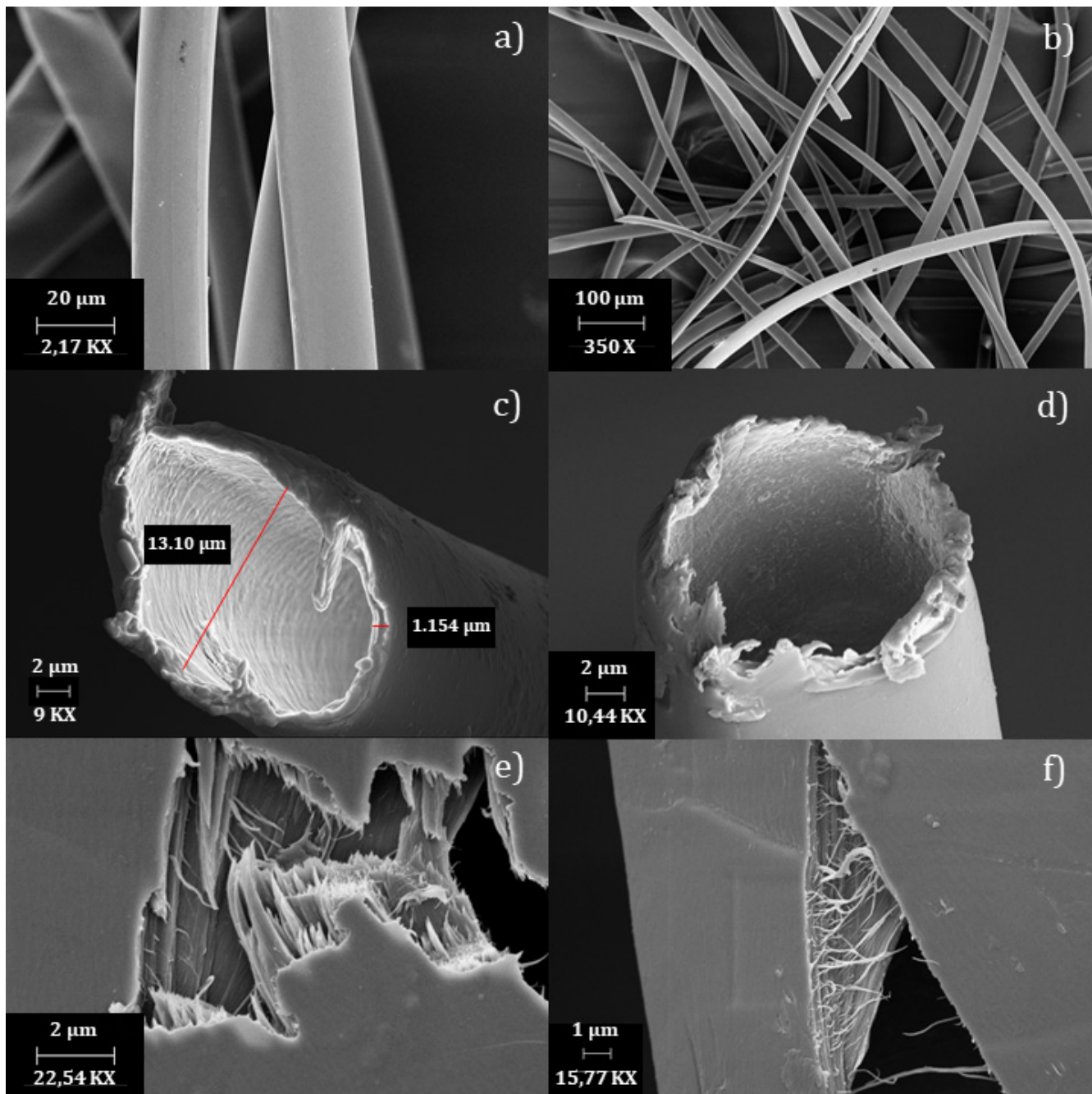

Figure 3. SEM images of IN sample. (**a**,**b**): overview of in natura fibers; (**c**,**d**): focus on tubular extremity of IN sample; (**e**,**f**): sites where there were ruptures.

The bands at 1597 cm^{-1} and 1503 cm^{-1} (C=C of lignin) [46,50,55,60] presented in the IN sample completely disappeared in the PU sample. On the other hand, the bands at 1739 cm^{-1} (C=O stretching of lignin and hemicellulose fractions) [55,59,61], 1463 cm^{-1} (CH$_3$ of lignin) [19,62] and 1246 cm^{-1} (C-O of lignin) [55,59,63] were still observed. However, their intensities were considerably reduced: the first two bands presented only a discrete shoulder in the PU sample spectrum, indicating that the lignin was not completely removed. This fact may be explained by the difficulty of isolating pure cellulose from vegetable

sources due to the complex chemical composition of lignin. This point was explored in the TG/dTG and DSC analysis. The bands at 1337 cm^{-1}, 1327 cm^{-1} and 1282 cm^{-1} (CH$_2$ wagging and C–O aromatic ring of cellulose) [55,59,62,63] were more evident in the PU sample, as well as the bands at 1429 cm^{-1} (CH$_2$ symmetrical band) and 897 cm^{-1} (β-glycosidic linkages between glucose units of cellulose) [24,46,63].
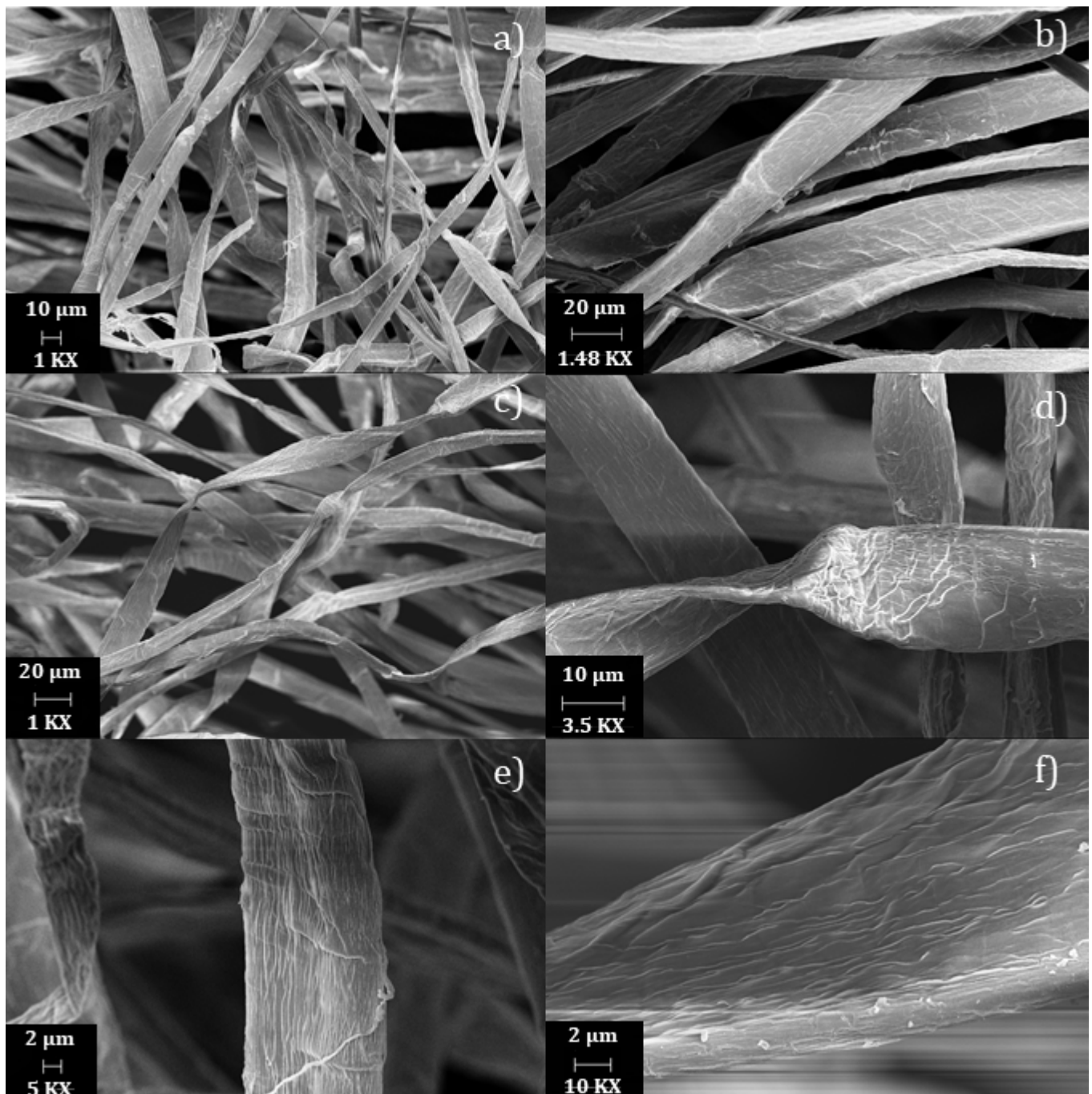

Figure 4. SEM images of PU sample. (**a**,**b**): Overview of cellulosic pulp; (**c**,**d**): sites where there were flexures in helix; (**e**,**f**): amplified view of rough surface of PU sample.
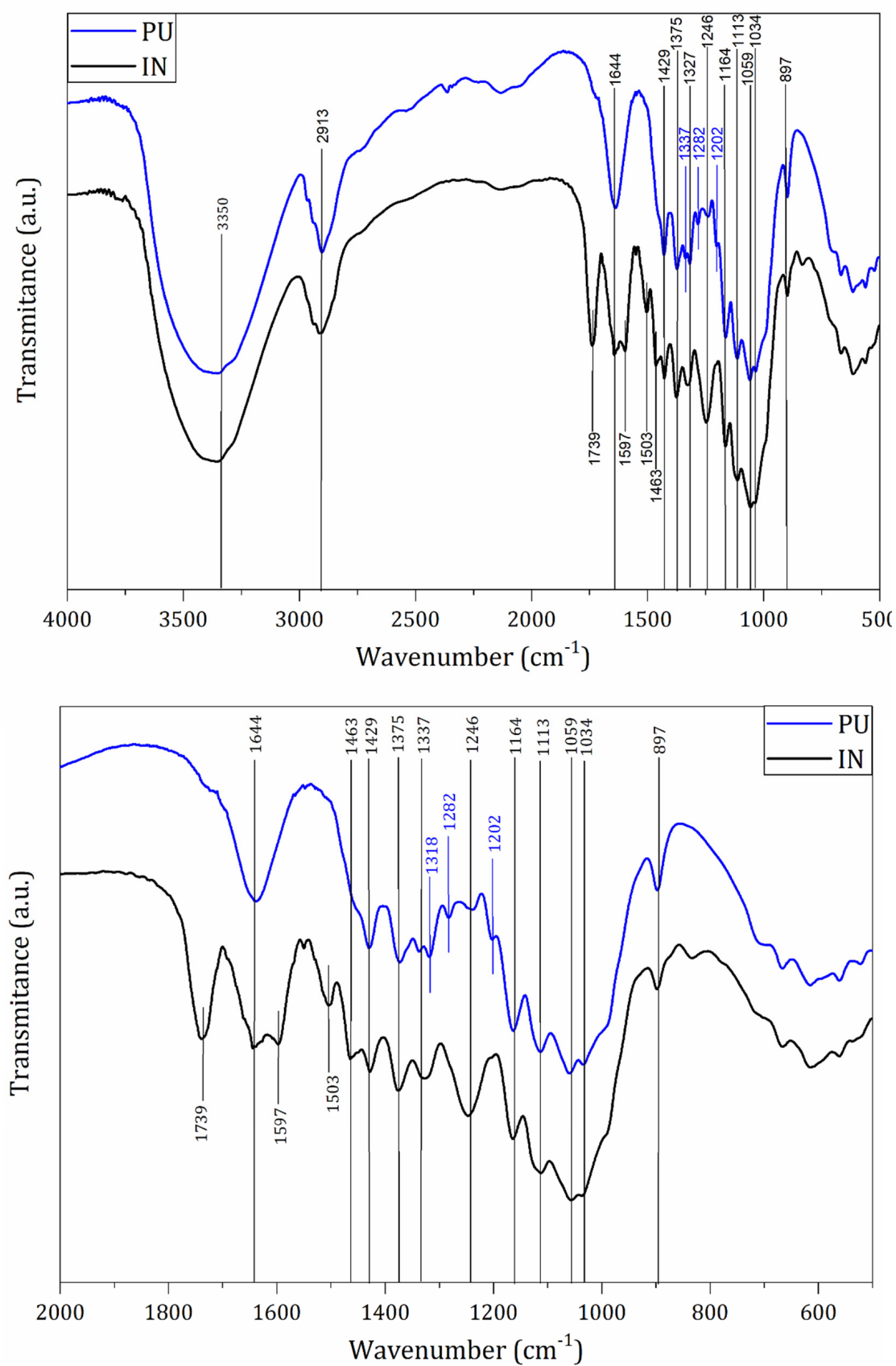
Figure 5. FTIR spectra recorded in the range of 4000–500 cm^{-1} for IN and PU samples.

Table 3. Vibrations modes from the FTIR spectra of IN and PU samples.

Wavenumber (cm^{-1})	Vibrational Modes	References
3350	O–H groups of cellulose or moisture	[19,62,64]
2913	C–H stretching	[47,64]
1739	C=O stretching of lignin and hemicellulose fractions	[55,59,61]
1644	Adsorbed water	[23,46,55]
1597/1503	C=C stretching of aromatic ring of lignin	[46,55,60]
1463	CH$_3$ deformation of lignin	[60,62]
1429	CH$_2$ symmetrical bending of cellulose	[24,46,47,63]
1375	C–H bending	[46,61]
1337/1327/1282	CH$_2$ wagging vibration and C–O aromatic ring of cellulose	[55,59,62,63]
1246	C–O stretching of lignin	[47,55,63]
1202/1164/1113/ 1059/1034	Multiple peaks of C–O–C pyranose ring	[30,61,62]
897	β-glycosidic linkages between glucose units of cellulose	[24,46,63]

3.5. TG/dTG Analysis

Lignocellulosic fibers present cellulose, hemicellulose and lignin as main components. For this reason, the thermal behavior depends on the concentration, individual characteristics and interaction of these components during pyrolysis [49,65]. Curves of TG/dTG of both IN and PU samples are shown in Figure 6a.

Considering the IN sample, the first thermal event ranged from 22 °C to 100 °C and was assigned to water release, resulting in 9% of mass loss [44,60,62]. The second thermal event was observed between 213 °C and 363 °C, and was attributed to the hemicellulose followed by cellulose decompositions, resulting in 54% of mass loss [66,67]. The hemicellulose degradation was observed before the cellulose decomposition, because the former is composed of multiple noncrystalline polysaccharides (such as xilans, arabinosis and galactans) presenting low-energy activation [49,59]. The third thermal event occurred between 363 °C and 526 °C and was attributed to the lignin decomposition and residual components, resulting in 35% of mass loss, a similar value found in the composition analysis shown in Table 1. The large temperature range of lignin decomposition is related to its molecular structure consisting of a complex network of cross-linked aromatic molecules resulting in high thermal stability [67]. The IN sample presented a remaining sample mass of 2%, as reported previously [19,52].

Considering the PU sample, the first thermal event was also related to the moisture release, occurring from 20 °C to 100 °C. The second thermal event was assigned to cellulose and residual hemicellulose degradation, which started at 235 °C, resulting in 63% of mass loss. This was the main observed thermal event, because cellulose represents the major component, resulting in the breaking of C–C and C–H bonds, saccharides carbonization [48], as well as releasing of CO, CO$_2$, CH$_4$ and H$_2$ [67]. The associated dTG curve presented the largest and narrowest peak with a maximum at 339 °C. The degradation range of cellulose is commonly reported between 280 °C and 360 °C [49]. Cellulose is more resistant to decomposition than hemicellulose due to its semicrystalline structure. However, after it started, it shows a high decomposition rate in a short temperature range, representing a typical pyrolysis behavior of linear polymers [65]. Finally, the third thermal event was initiated at 364 °C and assigned to residual lignin and other components degradation. The obtainment of pure cellulose continues to be a significant challenge due to the complex

molecular structure of lignin, as observed in this work by FTIR and thermal analysis. The lignin degradation is reported in the range of 100 and 900 °C, but its pyrolysis occurs mainly around 380 °C or at higher temperatures [49,67].
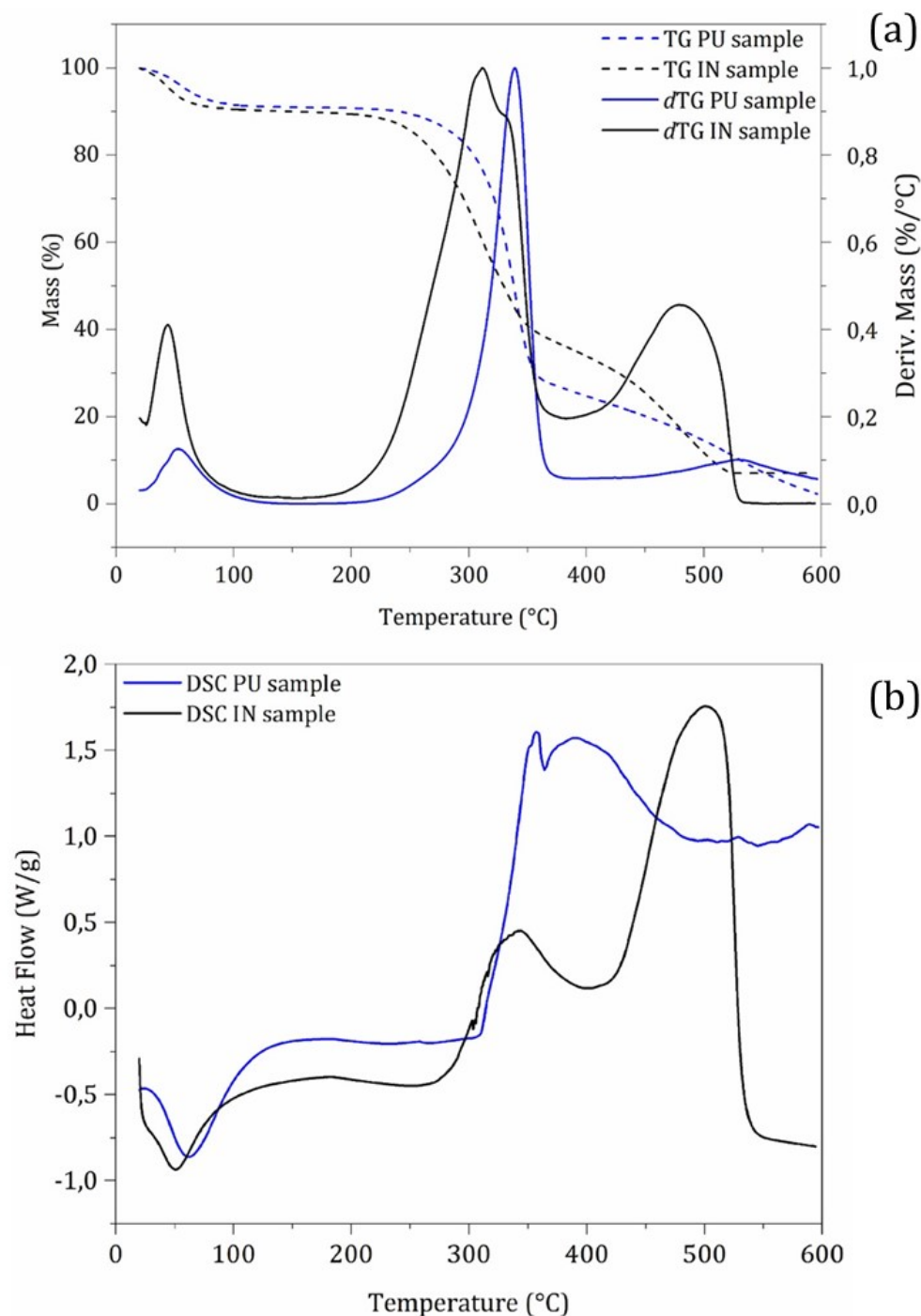

Figure 6. (**a**): TG/*d*TG and (**b**): DSC curves in the range of 20–600 °C obtained for IN and PU samples.

3.6. DSC Analysis

The DSC curves (Figure 6b) allowed for verifying the heat flow as a function of sample mass (W/g). All events and results were related to TG/*d*TG events. Therefore, the first thermal event of both IN and PU samples was assigned to the moisture release, occurring between 20 °C and 100 °C. The endothermic minimum peaks were observed at 50 °C in the IN sample and 62 °C in the PU sample [67]. The second thermal event was exothermic

and represented simultaneously the degradation of the main compounds, hemicellulose and cellulose. The presence of hemicellulose within a cellulosic sample extracted from lignocellulosic material is always subtle, and it may not be completely removed during the bleaching process. For this reason, the presence of hemicellulose was also observed in the DSC and FTIR results. The third thermal event was also exothermic, with the maximum peaks at 500 °C and 391 °C in the IN and PU samples, respectively, evidencing the degradation of lignin as well as residual components. The IN sample presented the most evident third thermal event, showing the necessity of higher energy for degradation due to the structural complexity and high amount of lignin. In the PU sample, the third event occurred in a temperature range prior to that observed in the IN sample due to the reduced amount of lignin, as well as the fact that its structure was already exposed as a consequence of the previous chemical treatment. This fact allowed for faster degradation. After the third event, other smaller peaks were observed and may be related to the decomposition of carbonization by-products [47], [68]. Table 4 summarizes the thermal events (TG/dTG and DSC curves) in the range of 20–600 °C obtained for IN and PU samples.

Table 4. Analysis of TG/dTG and DSC curves in the range of 20–600 °C obtained for IN and PU samples.

	IN Sample		
	1st Event	**2nd Event**	**3rd Event**
Temperature range (°C)	22–100	213–363	363–526
Mass loss (%)	9	54	35
T_{max} dTG (°C)	47	314	490
DSC effect/temperature (°C)	Endo/50 °C	Exo/343 °C	Exo/500 °C
	Remaining sample mass = 2.0%		
	PU sample		
	1st Event	**2nd Event**	**3rd Event**
Temperature range (°C)	20–100	235–364	364–600
Mass loss (%)	8.8	63.0	26.0
T_{max} dTG (°C)	52	339	529
DSC effect/temperature (°C)	Endo/62 °C	Exo/357 °C	Exo/391 °C
	Remaining sample mass = 2.2%		

3.7. Thermal Conductivity

The thermal conductivity values are shown in Table 5. The analysis was realized comparing the IN sample to cotton and EPS, materials already known as traditional insulating, and it was observed that the IN sample presented a lower value than the comparatives, indicating that *O. pyramidale* microfibers have excellent thermal insulating properties to be mainly explored as substitutes to nonbiodegradable and petroleum-based ones [69,70]. It is interesting to point out that the result of the IN sample was comparable to cellulose, cork and wood fiber, but with the advantage of being a fiber harvested from the fruit, which makes it an even more sustainable material since it is not necessary to destroy the complete individual and does not require chemical treatment to obtain it.

The thermal conductivity depends on the mean temperature difference of material, moisture content, porosity and density, and the *O. pyramidale* microfibers have very low density, even lower than cotton, a fact that contributes significantly to the insulating property, preventing the air movement, which provides the thermal resistance; thus, less material is needed to produce the same [71].

Table 5. Values of thermal conductivity of the IN sample, cotton, EPS and their comparison with referential values.

Material	Thermal Conductivity (W/m·K)	References
O. pyramidale fibers	0.036	Current work
Cotton	0.06	Current work
EPS	0.44	Current work
Cork	0.23–0.406	[71]
Cellulose	0.031	
Bamboo	0.077–0.088	[51]
Corn	0.101–0.139	
Hemp	0.039–0.123	
Kenaf	0.026–0.044	
Sunflower	0.038–0.05	
Rice husk	0.048–0.08	
Cotton	0.058–0.082	
Pineapple	0.035–0.057	
Wood fiber	0.038–0.05	

4. Conclusions

The physicochemical characterization of the *O. pyramidale* fiber revealed that it is constituted mainly by lignocellulosic components and extractives. This study suggests that the pulp extraction using the conventional method is feasible; however, the α-cellulose isolation step causes changes in its original structure, and, depending on the application, it can be dispensed, like in textile, paper, pharmaceutical and cosmetic industries, where its atomic arrangement is not the focus. Therefore, it is suggested that new more ecological routes for the extraction of cellulosic pulp be explored, aiming at the quality and yield of pulp while reducing steps and the use of polluting reagents. On the other hand, it is possible to explore different treatments to obtain different crystalline structures. The tubular morphology of this microfiber is its great differential, as it naturally has a format and dimension that are much sought after in research, such as for carrying bioactive matter. Moreover, it was found that this same characteristic gives microfiber the property of being a thermal insulator as efficient as other materials already used, with the advantages of being biodegradable and from a renewable source. It is expected that this paper will provide a fuse of necessary data for the wide range of research possibilities with this microfiber.

Author Contributions: Conceptualization, A.L.F.R. and E.A.S.; data analysis, A.L.F.R. and S.M.d.S.; formal analysis, A.L.F.R., B.d.A.F., A.d.S.C., R.Z.d.A.N., C.M.A.M., K.A.d.S., C.O.D. and S.M.d.S.; funding acquisition, E.A.S.; investigation, A.L.F.R., B.d.A.F., A.d.S.C., R.Z.d.A.N., C.M.A.M., K.A.d.S. and C.O.D.; methodology, A.L.F.R., B.d.A.F., A.d.S.C., R.Z.d.A.N., C.M.A.M., K.A.d.S., C.O.D. and S.M.d.S.; resources, A.L.F.R.; supervision, E.A.S.; validation, B.d.A.F., A.d.S.C., R.Z.d.A.N., C.M.A.M., K.A.d.S. and C.O.D.; writing—original draft, A.L.F.R., S.M.d.S. and E.A.S.; writing—review and editing, A.L.F.R., P.H.C., J.d.A.B. and E.A.S. All authors have read and agreed to the published version of the manuscript.

Conflicts of Interest: The authors declare no conflict of interest.

References

1. Dawit, J.B.; Regassa, Y.; Lemu, H.G. Property characterization of Acacia tortilis for natural fiber reinforced polymer composite. *Results Mater.* **2020**, *5*, 100054. [CrossRef]
2. Khan, A.S.; Man, Z.; Bustam, M.A.; Nasrullah, A.; Ullah, Z.; Sarwono, A.; Shah, F.U.; Muhammad, N. Efficient conversion of lignocellulosic biomass to levulinic acid using acidic ionic liquids. *Carbohydr. Polym.* **2018**, *181*, 208–214. [CrossRef]
3. Du, H.; Liu, W.; Zhang, M.; Si, C.; Zhang, X.; Li, B. Cellulose nanocrystals and cellulose nanofibrils based hydrogels for biomedical applications. *Carbohydr. Polym.* **2019**, *209*, 130–144. [CrossRef]
4. Li, Z.; Liu, W.; Guan, F.; Li, G.; Song, Z.; Yu, D.; Wang, H.; Liu, H. Using cellulose fibers to fabricate transparent paper by microfibrillation. *Carbohydr. Polym.* **2019**, *214*, 26–33. [CrossRef]
5. Leão, N.; de Freitas, A.D.D. Informativos Técnico Rede de Sementes da Amazônia Pau-de-balsa. *Rede Sementes Amazônia.* **2008**, 17–19. Available online: https://ainfo.cnptia.embrapa.br/digital/bitstream/item/173038/1/19-Pau-de-balsa.pdf (accessed on 29 June 2023).
6. Borrega, M.; Ahvenainen, P.; Serimaa, R.; Gibson, L. Composition and structure of balsa (Ochroma pyramidale) wood. *Wood Sci. Technol.* **2015**, *49*, 403–420. [CrossRef]
7. Malek, S.; Gibson, L.J. Multi-scale modelling of elastic properties of balsa. *Int. J. Solids Struct.* **2017**, *113*, 118–131. [CrossRef]
8. Masselter, T.; Kempe, A.; Caliaro, S.; Neinhuis, C.; Speck, T. Comparing structure and biomechanics of extant Carica papaya and Ochroma pyramidale stems allows re-evaluating the functional morphology of the fossil 'seed fern' Lyginopteris oldhamia. *Rev. Palaeobot. Palynol.* **2017**, *246*, 258–263. [CrossRef]
9. Santos, D.G.D.J.; Deuner, C.; De Almeida, A.P.F.; Meneghello, G.E.; Xavier, F.D.M. Superação de dormência em sementes de pau de balsa (Ochroma pyramidale). *Rev. Verde Agroecol. E Desenvolv. Sustentável* **2016**, *11*, 18. [CrossRef]
10. Rezende, G.M.; Vieira, D.L.M. Forest restoration in southern Amazonia: Soil preparation triggers natural regeneration. *For. Ecol. Manag.* **2019**, *433*, 93–104. [CrossRef]
11. Lim, T.T.; Huang, X. Evaluation of kapok (*Ceiba pentandra* (L.) Gaertn.) as a natural hollow hydrophobic-oleophilic fibrous sorbent for oil spill cleanup. *Chemosphere* **2007**, *66*, 955–963. [CrossRef]
12. Pooja, S.; Anbarasan, B.; Ponnusami, V.; Arumugam, A. Efficient production and optimization of biodiesel from kapok (Ceiba pentandra) oil by lipase transesterification process: Addressing positive environmental impact. *Renew. Energy* **2021**, *165*, 619–631. [CrossRef]
13. Tye, Y.Y.; Lee, K.T.; Wan Abdullah, W.N.; Leh, C.P. Potential of *Ceiba pentandra* (L.) Gaertn. (kapok) fiber as a resource for second generation bioethanol: Parametric optimization and comparative study of various pretreatments prior enzymatic saccharification for sugar production. *Bioresour. Technol.* **2013**, *140*, 10–14. [CrossRef]
14. Wang, J.; Zheng, Y.; Wang, A. Investigation of acetylated kapok fibers on the sorption of oil in water. *J. Environ. Sci.* **2013**, *25*, 246–253. [CrossRef] [PubMed]
15. Zheng, Y.; Wang, J.; Zhu, Y.; Wang, A. Research and application of kapok fiber as an absorbing material: A mini review. *J. Environ. Sci. (China)* **2015**, *27*, 21–32. [CrossRef]
16. Purnawati, R.; Febrianto, F.; Wistara, I.N.J.; Nikmatin, S.; Hidayat, W.; Lee, S.H.; Kim, N.H. Physical and chemical properties of kapok (Ceiba pentandra) and balsa (ochroma pyramidale) fibers. *J. Korean Wood Sci. Technol.* **2018**, *46*, 393–401. [CrossRef]
17. Prachayawarakorn, J.; Chaiwatyothin, S.; Mueangta, S.; Hanchana, A. Effect of jute and kapok fibers on properties of thermoplastic cassava starch composites. *Mater. Des.* **2013**, *47*, 309–315. [CrossRef]
18. Peraza-Ku, S.A.; Escobar-Morales, B.; Rodríguez-Fuentes, N.; Cervantes-Uc, J.M.; Uribe-Calderon, J.A. Ceiba pentandra cellulose crosslinked with citric acid for drug release systems. *Carbohydr. Res.* **2021**, *504*, 108334. [CrossRef] [PubMed]
19. Demosthenes, L.C.D.C.; Nascimento, L.F.C.; Monteiro, S.N.; Costa, U.O.; Filho, F.D.C.G.; da Luz, F.S.; Oliveira, M.S.; Ramos, F.J.H.T.V.; Pereira, A.C.; Braga, F.O. Thermal and structural characterization of buriti fibers and their relevance in fabric reinforced composites. *J. Mater. Res. Technol.* **2020**, *9*, 115–123. [CrossRef]
20. Mercedes, L.; Gil, L.; Bernat-Maso, E. Mechanical performance of vegetal fabric reinforced cementitious matrix (FRCM) composites. *Constr. Build. Mater.* **2018**, *175*, 161–173. [CrossRef]
21. Olacia, E.; Pisello, A.L.; Chiodo, V.; Maisano, S.; Frazzica, A.; Cabeza, L.F. Sustainable adobe bricks with seagrass fibres. Mechanical and thermal properties characterization. *Constr. Build. Mater.* **2020**, *239*, 117669. [CrossRef]
22. ben Hammouda, S.; Chen, Z.; An, C.; Lee, K. Recent advances in developing cellulosic sorbent materials for oil spill cleanup: A state-of-the-art review. *J. Clean. Prod.* **2021**, *311*, 127630. [CrossRef]
23. Cardoso, C.K.M.; Mattedi, S.; Lobato, A.K.D.C.L.; Moreira, T.A. Remediation of petroleum contaminated saline water using value-added adsorbents derived from waste coconut fibres. *Chemosphere* **2021**, *279*, 130562. [CrossRef]
24. Aguilar, N.M.; Arteaga-Cardona, F.; de Anda Reyes, M.E.; Gervacio-Arciniega, J.J.; Salazar-Kuri, U. Magnetic bioplastics based on isolated cellulose from cotton and sugarcane bagasse. *Mater. Chem. Phys.* **2019**, *238*, 121921. [CrossRef]
25. Gallardo-Rodríguez, J.J.; Rios-Rivera, A.C.; Von Bennevitz, M.R. Living biomass supported on a natural-fiber biofilter for lead removal. *J. Environ. Manag.* **2019**, *231*, 825–832. [CrossRef]
26. Nagarajan, S.; Skillen, N.C.; Irvine JT, S.; Lawton, L.A.; Robertson PK, J. Cellulose II as bioethanol feedstock and its advantages over native cellulose. *Renew. Sustain. Energy Rev.* **2017**, *77*, 182–192. [CrossRef]
27. Pal, R.K.; Goyal, P.; Sehgal, S. Effect of cellulose fibre based insulation on thermal performance of buildings. *Mater. Today Proc.* **2021**, *45*, 5778–5781. [CrossRef]

28. Piégay, C.; Glé, P.; Gourdon, E.; Gourlay, E.; Marceau, S. Acoustical model of vegetal wools including two types of fibers. *Appl. Acoust.* **2018**, *129*, 36–46. [CrossRef]

29. Abou-Yousef, H.; Dacrory, S.; Hasanin, M.; Saber, E.; Kamel, S. Biocompatible hydrogel based on aldehyde-functionalized cellulose and chitosan for potential control drug release. *Sustain. Chem. Pharm.* **2021**, *21*, 100419. [CrossRef]

30. Soliman, M.; Sadek, A.A.; Abdelhamid, H.N.; Hussein, K. Graphene oxide-cellulose nanocomposite accelerates skin wound healing. *Res. Vet. Sci.* **2021**, *137*, 262–273. [CrossRef]

31. Morais, J.P.S.; Rosa, M.D.F.; Marconcini, J.M. *Procedimentos Para Análise Lignocelulósica*; EMBRAPA: Brasilia, Brazil, 2010.

32. TAPPI. *T 211 om-02 Ash in Wood Pulp Paper Paperboard: Combustion at 525 °C*; Technical Association of the Pulp and Paper Industry: Tokyo, Japan, 2017; pp. 525–530. [CrossRef]

33. TAPPI. *T 207 cm-99 Water Solubility of Wood and Pulp*; Technical Association of the Pulp and Paper Industry: Tokyo, Japan, 1999; pp. 6–8. [CrossRef]

34. TAPPI. *T 204 cm-97 Solvent Extractives of Wood and Pulp*; Technical Association of the Pulp and Paper Industry: Tokyo, Japan, 2007; pp. 7–10.

35. TAPPI. *T 222 om-02 Lignin in Wood and Pulp*; Technical Association of the Pulp and Paper Industry: Tokyo, Japan, 2011; pp. 1–7. [CrossRef]

36. TAPPI. *T 203 cm-99 Alpha-, Beta- and Gamma-Cellulose in Pulp*; Technical Association of the Pulp and Paper Industry: Tokyo, Japan, 1999; pp. 5–9.

37. Mccusker, L.B.; Von Dreele, R.B.; Cox, D.E.; Louër, D.; Scardi, P. Rietveld refinement guidelines. *J. Appl. Crystallogr.* **1999**, *32*, 36–50. [CrossRef]

38. Nishiyama, Y.; Sugiyama, J.; Chanzy, H.; Langan, P. Crystal Structure and Hydrogen Bonding System in Cellulose Iα from Synchrotron X-ray and Neutron Fiber Diffraction. *J. Am. Chem. Soc.* **2003**, *125*, 14300–14306. [CrossRef]

39. Langan, P.; Nishiyama, Y.; Chanzy, H. X-ray structure of mercerized cellulose II at 1 Å resolution. *Biomacromolecules* **2001**, *2*, 410–416. [CrossRef]

40. Biondo, M.M.; de Oliveira, L.M.; Lima, S.X.; de Souza Carolino, A.; Rocha AL, F.; da Silva, J.P.; Sanches, E.A. Chemically synthesized poly(o-methoxyaniline): Influence of counterions on the structural and electrical properties. *J. Mol. Struct.* **2020**, *1205*, 127588. [CrossRef]

41. Veras, T.N.; Carolino, A.S.; Lima, S.X.; Biondo, M.M.; Santos, N.A.; Campelo, P.H.; Ruiz, Y.L.; Frota, H.O.; Sanches, E.A. Characterization and DFT calculation of poly(m-anisidine) synthesized with different dopant acids. *J. Mol. Struct.* **2020**, *1201*, 127182. [CrossRef]

42. Götz, A.; Senz, V.; Schmidt, W.; Huling, J.; Grabow, N.; Illner, S. General image fiber tool: A concept for automated evaluation of fiber diameters in SEM images. *Meas. J. Int. Meas. Confed.* **2021**, *177*, 109265. [CrossRef]

43. Sridhar, K.; Charles, A.L. In vitro antioxidant activity of Kyoho grape extracts in DPPH [rad] and ABTS [rad] assays: Estimation methods for EC 50 using advanced statistical programs. *Food Chem.* **2019**, *275*, 41–49. [CrossRef]

44. Guna, V.; Ilangovan, M.; Adithya, K.; Akshay, A.K.; Srinivas, C.V.; Yogesh, S.; Nagananda, G.S.; Venkatesh, K.; Reddy, N. Biofibers and biocomposites from sabai grass: A unique renewable resource. *Carbohydr. Polym.* **2019**, *218*, 243–249. [CrossRef] [PubMed]

45. Alotaibi, M.D.; Alshammari, B.A.; Saba, N.; Alothman, O.Y.; Sanjay, M.R.; Almutairi, Z.; Jawaid, M. Characterization of natural fiber obtained from different parts of date palm tree (*Phoenix dactylifera* L.). *Int. J. Biol. Macromol.* **2019**, *135*, 69–76. [CrossRef]

46. Kian, L.K.; Jawaid, M.; Ariffin, H.; Alothman, O.Y. Isolation and characterization of microcrystalline cellulose from roselle fibers. *Int. J. Biol. Macromol.* **2017**, *103*, 931–940. [CrossRef] [PubMed]

47. Kathirselvam, M.; Kumaravel, A.; Arthanarieswaran, V.P.; Saravanakumar, S.S. Isolation and characterization of cellulose fibers from Thespesia populnea barks: A study on physicochemical and structural properties. *Int. J. Biol. Macromol.* **2019**, *129*, 396–406. [CrossRef]

48. Spinacé, M.A.S.; Lambert, C.S.; Fermoselli, K.K.G.; De Paoli, M.A. Characterization of lignocellulosic curauá fibres. *Carbohydr. Polym.* **2009**, *77*, 47–53. [CrossRef]

49. Stefanidis, S.D.; Kalogiannis, K.G.; Iliopoulou, E.F.; Michailof, C.M.; Pilavachi, P.A.; Lappas, A.A. A study of lignocellulosic biomass pyrolysis via the pyrolysis of cellulose, hemicellulose and lignin. *J. Anal. Appl. Pyrolysis* **2014**, *105*, 143–150. [CrossRef]

50. Kuznetsov, B.N.; Chudina, A.I.; Kazachenko, A.S.; Fetisova, O.Y.; Borovkova, V.S.; Vorobyev, S.A.; Karacharov, A.A.; Gnidan, E.V.; Mazurova, E.V.; Skripnikov, A.M.; et al. Fractionation of Aspen Wood to Produce Microcrystalline, Microfibrillated and Nanofibrillated Celluloses, Xylan and Ethanollignin. *Polymers* **2023**, *15*, 2671. [CrossRef]

51. Kumar, P.S.S.; Allamraju, K.V. A review of natural fiber composites [Jute, Sisal, Kenaf]. *Mater. Today Proc.* **2019**, *18*, 2556–2562. [CrossRef]

52. Kathirselvam, M.; Kumaravel, A.; Arthanarieswaran, V.P.; Saravanakumar, S.S. Assessment of cellulose in bark fibers of Thespesia populnea: Influence of stem maturity on fiber characterization. *Carbohydr. Polym.* **2019**, *212*, 439–449. [CrossRef]

53. Feitosa, B.d.A.; Rocha AL, F.; Lima, S.X.; de Oliveira, L.M.; Biondo, M.M.; Campelo, P.H.; Sanches, E.A. Nanocomposites based on the cellulose extracted from the Amazon Peperomia pellucida and polyaniline derivatives: Structural and thermal properties. *Chem. Pap.* **2020**, *75*, 1809–1821. [CrossRef]

54. French, A.D. Idealized powder diffraction patterns for cellulose polymorphs. *Cellulose* **2014**, *21*, 885–896. [CrossRef]

55. Zhang, Z.; Zhu, M.; Zhang, D. Pyrolysis Characteristics of Cellulose Isolated from Selected Biomass Feedstocks using a Thermogravimetric Analyser. *Energy Procedia* **2017**, *142*, 636–641. [CrossRef]

56. Ju, X.; Bowden, M.; Brown, E.E.; Zhang, X. An improved X-ray diffraction method for cellulose crystallinity measurement. *Carbohydr. Polym.* **2015**, *123*, 476–481. [CrossRef]
57. Faria LU, S.; Pacheco BJ, S.; Oliveira, G.C.; Silva, J.L. Production of cellulose nanocrystals from pineapple crown fibers through alkaline pretreatment and acid hydrolysis under different conditions. *J. Mater. Res. Technol.* **2020**, *9*, 12346–12353. [CrossRef]
58. Bajpai, P. *Carbon Fibre from Lignin*; Springer: Singapore, 2017. [CrossRef]
59. Kumneadklang, S.; O-Thong, S.; Larpkiattaworn, S. Characterization of cellulose fiber isolated from oil palm frond biomass. *Mater. Today Proc.* **2019**, *17*, 1995–2001. [CrossRef]
60. Lin, Q.; Huang, Y.; Yu, W. Effects of extraction methods on morphology, structure and properties of bamboo cellulose. *Ind. Crops Prod.* **2021**, *169*, 113640. [CrossRef]
61. Caputo, D.; Fusco, C.; Nacci, A.; Palazzo, G.; Murgia, S.; D'Accolti, L.; Gentile, L. A selective cellulose/hemicellulose green solvents extraction from buckwheat chaff. *Carbohydr. Polym. Technol. Appl.* **2021**, *2*, 100094. [CrossRef]
62. Manzato, L.; Rabelo LC, A.; de Souza, S.M.; da Silva, C.G.; Sanches, E.A.; Rabelo, D.; Mariuba LA, M.; Simonsen, J. New approach for extraction of cellulose from tucumã's endocarp and its structural characterization. *J. Mol. Struct.* **2017**, *1143*, 229–234. [CrossRef]
63. Devnani, G.L.; Sinha, S. Extraction, characterization and thermal degradation kinetics with activation energy of untreated and alkali treated Saccharum spontaneum (Kans grass) fiber. *Compos. Part B Eng.* **2019**, *166*, 436–445. [CrossRef]
64. Leite AL, M.P.; Zanon, C.D.; Menegalli, F.C. Isolation and characterization of cellulose nanofibers from cassava root bagasse and peelings. *Carbohydr. Polym.* **2017**, *157*, 962–970. [CrossRef]
65. Yu, J.; Paterson, N.; Blamey, J.; Millan, M. Cellulose, xylan and lignin interactions during pyrolysis of lignocellulosic biomass. *Fuel* **2017**, *191*, 140–149. [CrossRef]
66. Peng, Y.; Wu, S. The structural and thermal characteristics of wheat straw hemicellulose. *J. Anal. Appl. Pyrolysis* **2010**, *88*, 134–139. [CrossRef]
67. Yang, H.; Yan, R.; Chen, H.; Lee, D.H.; Zheng, C. Characteristics of hemicellulose, cellulose and lignin pyrolysis. *Fuel* **2007**, *86*, 1781–1788. [CrossRef]
68. Zhao, J.; Xiuwen, W.; Hu, J.; Liu, Q.; Shen, D.; Xiao, R. Thermal degradation of softwood lignin and hardwood lignin by TG-FTIR and Py-GC/MS. *Polym. Degrad. Stab.* **2014**, *108*, 133–138. [CrossRef]
69. Athayde, J.N.; Fernandes, B.L.; de Siqueira, C.J.M.; Nohama, P.; Fernandes, C.R. Device for in vitro wear analysis of biomaterials in the hinged prosthesis configuration. *Facta Univ. Ser. Mech. Eng.* **2018**, *16*, 381–388. [CrossRef]
70. Hurtado, P.L.; Rouilly, A.; Vandenbossche, V.; Raynaud, C. A review on the properties of cellulose fibre insulation. *Build. Environ.* **2016**, *96*, 170–177. [CrossRef]
71. Ijjada, N.; Nayaka, R.R. Review on properties of some thermal insulating materials providing more comfort in the building. *Mater. Today Proc.* **2022**, *58*, 1354–1359. [CrossRef]